


Research Article

Boosted Thermal Storage Performance of $\text{LiOH}\cdot\text{H}_2\text{O}$ by Carbon Nanotubes Isolated Multilayered Graphene Oxide Frames

Yuxian Wang,¹ Jing Gu,^{2,3} Xian Li ,¹ Yan Zhu,¹ Hongyun Hu,¹ Huan Liu,¹ Guangqian Luo,¹ and Hong Yao¹

¹State Key Laboratory of Coal Combustion, School of Energy and Power Engineering, Huazhong University of Science and Technology, Wuhan 430074, China

²Guangzhou Institute of Energy Conversion, Chinese Academy of Sciences, Guangzhou 510640, China

³Southern Marine Science and Engineering Guangdong Laboratory (Guangzhou), Guangzhou 510640, China

Correspondence should be addressed to Xian Li; xian_li@hust.edu.cn

Received 1 December 2021; Revised 2 February 2022; Accepted 7 February 2022; Published 11 March 2022

Academic Editor: Apostolos Avgeropoulos

Copyright © 2022 Yuxian Wang et al. This is an open access article distributed under the Creative Commons Attribution License, which permits unrestricted use, distribution, and reproduction in any medium, provided the original work is properly cited.

Cellulose-originated three-dimensional graphene oxide CNT-modified $\text{LiOH}\cdot\text{H}_2\text{O}$ (3D-GO-CNTs- $\text{LiOH}\cdot\text{H}_2\text{O}$) was synthesized by the hydrothermal method. $\text{LiOH}\cdot\text{H}_2\text{O}$ nanoparticles (5–50 nm) were homogeneously dispersed inside the 3D-GO-CNTs frames. The composite showed enhanced heat storage density, excellent thermal conductivity, and greatly improved hydration rate due to both the hydrophilic reaction interface of 3D-GO-CNTs frames and reduced size of $\text{LiOH}\cdot\text{H}_2\text{O}$ nanoparticles. $\text{LiOH}\cdot\text{H}_2\text{O}$ content ratio of 23% (3D-GO-CNTs- $\text{LiOH}\cdot\text{H}_2\text{O}$ -1) results in best heat storage performance with activation energy of 23.8 kJ/mol, thermal conductivity of 3.06 W/m-K, and heat storage capacity of 2800 kJ/kg. 3D-GO-CNTs- $\text{LiOH}\cdot\text{H}_2\text{O}$ shows 4.2 folders heat storage capacity than that of pristine $\text{LiOH}\cdot\text{H}_2\text{O}$ after the same hydration reaction. Other composite materials also show good performance: 3D-GO-CNTs- $\text{LiOH}\cdot\text{H}_2\text{O}$ -2 (activation energy: 28.5 kJ/mol, thermal conductivity: 2.33 W/m-K, and heat storage capacity: 2051 kJ/kg.); 3D-GO-CNTs- $\text{LiOH}\cdot\text{H}_2\text{O}$ -3 (activation energy: 32.3 kJ/mol, thermal conductivity: 2.01 W/m-K, and heat storage capacity: 1983 kJ/kg.). The addition of cellulose originated 3D-GO-CNTs was proved to be an excellent strategy to boost the heat storage performance of $\text{LiOH}\cdot\text{H}_2\text{O}$.

1. Introduction

Sharply increased fossil energy exhaustion and global warming could be effectively mitigated by reducing CO_2 emissions [1, 2]. Heat storage technology is one of the possible technologies to reduce CO_2 emissions [3–5]. This technology could be used both for the recovering of industrial waste energy and utilization of renewable energy including solar heat and wind-generated heat [6]. Sensible heat, latent heat, and thermochemical heat are three categories derived from the heat storage technology [7]. Among which, thermochemical heat generally bears the highest heat storage capacity while being confined by poor recyclability and thermal conductivity for industrial applications.

Many chemical heat storage materials have been previously reported [8–13]. Among these materials, most of

them were used for high temperature heat storage such as $\text{Mg}(\text{OH})_2$ and CaCO_3 . Ishitobi and other researchers [10] studied the dehydration and hydration behavior of $\text{Mg}(\text{OH})_2$. They used impregnation method to compose LiCl with $\text{Mg}(\text{OH})_2$ in order to decline the activation energy and reaction temperature to increasing the energy efficiency; finally, the dehydration temperature of modified $\text{LiCl}/\text{Mg}(\text{OH})_2$ decreased from 350°C to 280°C. Khosa et al. [11] used high temperature decomposition method to prepare CaCO_3/CaO as chemical heat storage material, and their results showed that the decarbonation temperature of CaCO_3 greatly influences the heat supply performance and adding of SiO_2 also showed obvious impact on the decarbonation temperature. The heat storage temperature range decreased from 750–925°C to 700–800°C. Both above two types of materials were used to store high temperature

thermal energy, and the price of these material was around 6.3 USA\$/kg, but these materials could not utilize low temperature thermal energy below 200°C. MgSO₄ as typical low temperature thermal energy storage material could store heat at the range of 122–150°C [12] and the heat storage density could reach 1200 kJ/kg, but it could always form a dense surface, which cover the core material and block the further reaction; hence, various additives were used to modify it and get better materials such as zeolite/MgSO₄ [9]. The price of MgSO₄ could reach 2.4 USA\$/kg. Lithium hydroxide monohydrate (LiOH·H₂O) was recently applied to store low temperature thermal energy owing to its high energy density (1400 kJ/kg) and mild reaction conditions (30°C) [14]. It could store the low temperature thermal energy at the range of 80–100°C [15], which was lower than MgSO₄ and the heat storage density was higher than it. Its price was about 7.5 USA\$/kg. While like other inorganic hydrate materials [16, 17], poor hydration reaction rate, low thermal conductivity [12, 14], and quickly degenerated heat storage capability of LiOH·H₂O after repeated hydration reactions critically limited its industrial application.

Three-dimensional (3D) carbon nanotube sponge, arrays [18], and graphene [19–21] with excellent physical-chemical stability [22–25] were widely applied in electronics [26–28] and catalysis [29, 30].

Among them the grapheme-type materials have attracted great attention. And, various synthesis methods have been developed. Carbon sources, environment, and synthesis approach have been considered as the most important factors for graphene preparation. The main graphene preparing methods contained epitaxial growth, liquid-phase chemical/electrochemical exfoliation, mechanical exfoliation chemical vapor deposition [31], and microwave-assisted synthesis [32]. Graphene composed with metal oxides and metal sulphides can be used for electrodes in Li-ion batteries. Besides, laser-assisted synthesis was also an excellent method for graphene preparation. For example, direct laser writing enables local graphene synthesis and fabrication of graphene patterns on graphene oxide films. It can be used for supercapacitors [33]. Heteroatom doping (B, N, P, and S) method decoration with nanoparticles and composite microstructures formation for modifications of graphene and rGO has been applied for supercapacitors, electrodes, fuel cells, and solar cells [34, 35].

Prof. Kumar et al. [36, 37] used microwave-assisted method to synthesize reduced graphene oxide-wrapped manganese cobaltite ternary hybrids and reduced graphene modified oxide-cobalt oxide nanoparticle hybrids as supercapacitor electrode. During the synthesis process of reduced graphene oxide-based material, the exfoliated effect of microwave was particularly important. It was found that rGO-NiCoO₂ composite prepared by the microwave-assisted method presented enhanced field emission performance and could apply for electron field emitter [38]. Their group also prepared graphene nanosheets-ZnO composite by solvothermal method accompanied with hydrothermal method and applied in electronic field [39]. Hashtroudi et al. [40] investigated the hydrogen gas sensing property of microwave-assisted two-dimensional rGO-based hybrid

material. The result showed that temperature, humidity, and UV illumination obviously influenced the hydrogen gas sensing property of this material, and it had great potential to manufacture sensitive hydrogen sensor. El-Hallag and other researchers [41] using in situ electrochemical reduction method synthesized a reduced graphene oxide nanosheets embedded palladium nanoparticles hybrids on Ni-sheet. This composite material could be used for supercapacitor electrode. Graphene-based composite materials could also be applied for microwave electromagnetic interference shielding due to its good absorption and reflection property of electromagnetic waves [42]. All above researches proved that graphene-based materials showed excellent property for potential applications in many technological fields. Therefore, in our research, graphene-based materials were chosen to synthesize and applied for thermal energy storage.

However, in order to get more positive effects on the environment by consuming fossil resources and complicated production, cellulose-based material was reported to be successfully fabricated into carbon nanotube (CNT) [43] and graphene oxide (GO) [44] for electronic devices and oil spill cleaning. Cellulose-based material was a better choice for 3D porous carbon frame due to its easy fabrication, abundant amount in nature, and safety for the environment [45]. In this work, 3D porous GO frames synthesized from green cellulose-based materials were applied as 3D-carbon frames for nanosized LiOH·H₂O. By further plugging the CNTs into the interlayers of 3D-GO frame, LiOH·H₂O can be more uniformly dispersed into 3D-GO frames. And, both the thermal conductivity perpendicular and parallel to the GO surface (Figure 1, indicated by the red arrow) could be enhanced. Finally, a highly desired composite with both good thermal conductivity and heat storage capacity was obtained.

2. Experimental

2.1. Materials. Microcrystalline cellulose and lithium hydroxide monohydrate were purchased from Aladdin Chemistry Co., Ltd. NaOH (AR, ≥96%), urea (AR, 99%), K₂S₂O₈ (AR, ≥99.5%), H₂O₂ (AR, 30%), phytic acid (50%), ascorbic acid (AR, 99%), and P₂O₅ (AR, ≥98.5%) were bought from Tianjin Damao Chemical Reagent Factory. H₂SO₄ (AR, ≥98%) and HCl (AR, 36–38%) were bought from Hui Hong Yuan Chemical Co., Ltd. CH₄ (≥99.99%) and N₂ (≥99.99%) were bought from Guangzhou Puyuan Gas Company Co., Ltd. All chemicals were used as received without any purification unless otherwise specified.

2.2. Preparation of Cellulose-Based 3D-GO-CNTs-Modified LiOH·H₂O Composites. The whole preparation procedure of cellulose-based 3D-GO-CNTs-modified LiOH·H₂O composite is shown in Figure 2. The catalytic chemical vapor deposition method (CCVD) followed by the hydrothermal method were applied to fabricate 3D-GO-CNTs-LiOH·H₂O.

Carbon nanotubes (CNTs) were synthesized by the CCVD method [15] using CH₄ and nickel foam as carbon

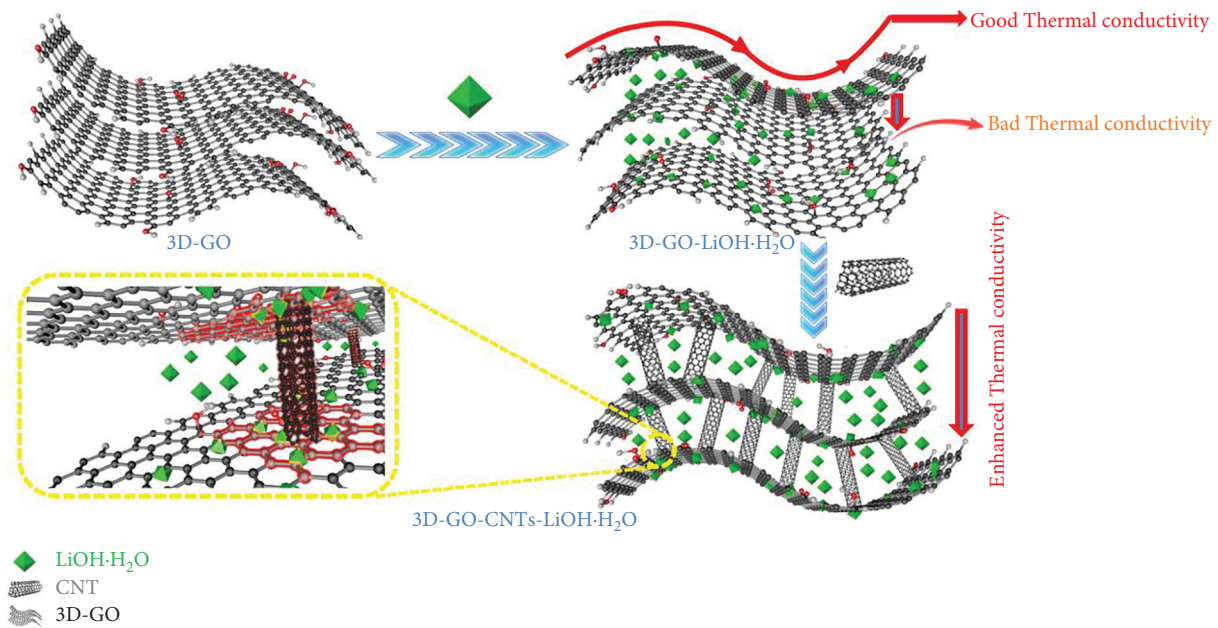


FIGURE 1: Enhanced thermal conductivity perpendicular to the GO surfaces.

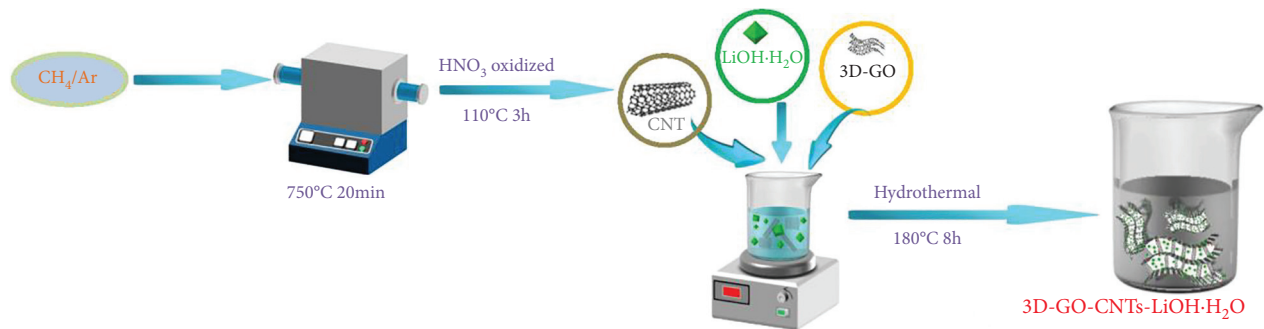


FIGURE 2: Preparation procedure of cellulose-based 3D-GO-CNTs-modified LiOH-H₂O composites.

source and catalyst, respectively. Firstly, the surface pre-oxidation of metal nickel foam was performed in a furnace at 700°C for 1 h. The nickel foam was then taken out and put into a tubular furnace. Mixed Ar/H₂ (150 mL/50 mL) gas was then charged into the furnace. Raised the furnace temperature to 700°C and kept for 2 h. After that, Ar/H₂ is replaced by Ar/CH₄ (200 mL/50 mL) and kept at 750°C for 20 min. Finally, the mixture was cooled down to 25°C and then oxidized in concentrated HNO₃ (AR, 98%) for 3 h at 110°C. Obtained black powders are CNTs.

Microcrystalline cellulose was used as a precursor to prepare 3D-GO. Firstly, NaOH, Urea and deionized water was mixed at a mole ratio of 7 : 8:180. In this mixture, NaOH, urea, and water formed an alkaline solvent, due to cellulose could only dissolve in alkaline solvent. The advantage effect of urea in synthesis process is to destroy the intramolecular hydrogen bond in alkaline solution, so the addition of urea is conducive to promote the dissolution of cellulose. This solution (200 mL) was then placed in an isopropyl alcohol bath and kept at -13°C. Then, 0.19 mol (30 g) cellulose powder was introduced into the solution under stirring (800 rpm) for 30 min. After centrifugal separation

(4000 rpm, 5 min), the temperature of the cellulose solution was raised to 60°C and kept for 5 h until a cellulose gel formed. The gel was continuously rinsed by distilled (DI) water until a pH value of 7 was reached. Then, the gel was dried in a vacuum freeze dryer at -50°C for 72 h. The obtained cellulose aerogel was transferred into a tubular furnace, and the temperature was raised to 600°C at a heating rate of 3°C/min in N₂ and kept for 2 h. Cellulose-based porous carbon was obtained [29]. Then, 0.50 mol (6 g) porous carbon, 1.10 mol concentrated sulfuric acid (H₂SO₄, 60 mL), 0.02 mol potassium persulfate (K₂S₂O₈, 5 g), and 0.04 mol phosphorus pentoxide (P₂O₅, 5 g) were mixed and reacted in an oven at 80°C for 5 h. After being cooled down, the solid mixture was separated and dried at 80°C. Then, this mixture was added into 4.42 mol concentrated sulfuric acid (240 mL) in a 500 mL beaker. Transferred the beaker to an ice bath and then 30 g KMnO₄ (0.19 mol) was added to the beaker under slow magnetic stirring. The reaction temperature should be lower than 30°C during the adding of KMnO₄. Kept this reaction for 2 h. 6.94 mol DI water (125 mL) was then added to dilute the reaction solution and kept stirring for another 2 h. Then, 22.22 mol DI water

(400 mL) was added followed by 40 mL 30% H₂O₂ solution (0.52 mol). The obtained mixture was washed by 10 vol.% HCl (14.58 mol; 5 L). Finally, the obtained GO solution was filled into a dialysis bag and then soaked in DI water bath. This DI water bath was refreshed twice a day and kept dialyzing for 7 d until the bath pH reached 7. The obtained concentration of the GO solution was 4 mg/mL. After that, the GO solution was concentrated to 10 mg/mL for further use [46].

Then, the CNTs were ultrasonicated in DI water for 30 min and mixed with GO solution (10 mg/mL) at a mass ratio of CNTs/GO of 0.25. Various amounts of LiOH·H₂O were then dissolved in this mixture under vigorous stirring. This dispersion was dispersed into a 250 mL hydrothermal reactor, heated to 180°C, and kept for 8 h. With the help of functional (hydroxyl, carbocyclic, and carboxyl on its surface and edges) group attached on the GO surfaces [47], when 3D-GO-CNTs-LiOH·H₂O was constructed in high temperature and high pressure water environment, GO sheets were constantly connected together to form 3D porous structure; meanwhile, CNTs and LiOH·H₂O were anchored and coated in these frames. After naturally cooling down to room temperature, the final products were collected and dried. The obtained composites were denoted as 3D-GO-CNTs-LiOH·H₂O-1, 3D-GO-CNTs-LiOH·H₂O-2, 3D-GO-CNTs-LiOH·H₂O-3, and LiOH·H₂O, according to various LiOH·H₂O contents (23, 39, 59, and 100 wt.%), respectively.

2.3. Characterizations. SEM (S-4800, Hitachi, Japan) and TEM (JEM-2100F, JEOL, Japan) was used to observe the morphology of the 3D-GO-CNTs-modified LiOH·H₂O composites. XRD (D8-advance X-ray diffractometer, Bruker, Germany) was applied to identify the crystallization phase of the sample. BET test was carried out on Quantachrome QDS-30 analyzer (QDS-30, Quantachrome, USA). Thermal conductivity tester (DRL-II, Xiangtan Xiangyi Instrument, China.) was chosen to test the thermal conductivity of all samples. LiOH·H₂O, 3D-GO-CNTs-LiOH·H₂O-1, 3D-GO-CNTs-LiOH·H₂O-2, and 3D-GO-CNTs-LiOH·H₂O-3 were decomposed separately in a horizontal tubular quartz furnace in N₂ atmosphere at 150°C for 5 h to synthesize LiOH, 3D-GO-CNTs-LiOH-1, 3D-GO-CNTs-LiOH-2, and 3D-GO-CNTs-LiOH-3, respectively. After the temperature of the formed materials was cooled down to 25°C, water steam together with N₂ gas was introduced into the furnace and reacted at 30°C for 60 min. Thereafter, TG-DSC (STA-200, Nanjingdazhan, China.) was used to test the heat change and the mass loss of the sample. Each TG-DSC test was performed thrice for accuracy. The dehydration reaction activation energy of the composite was calculated by Ozawa method [48–50] using the following equation:

$$\ln\left(\frac{\beta}{T^2}\right) = \ln \frac{R}{E} \frac{A}{f(\alpha)} - \frac{E}{R T} \quad (1)$$

E and β are the activation energy (kJ/mol) and heating rate (K/s), respectively. T is the temperature (K), R is the ideal gas constant (J/mol·K), A stands for pre-exponential factor, and α and $f(\alpha)$ are the dehydration conversion ratio

and dehydration conversion function, respectively. The activation energy was calculated by $-E/R$ at 70% dehydration conversion ratio, and the heating rates are 5, 7, and 10 K/min, respectively.

3. Results and Discussion

3.1. Microstructural Characterization. Figure 3 shows the XRD spectrum of LiOH·H₂O, 3D-GO-CNTs, 3D-GO-CNTs-LiOH·H₂O-1, 3D-GO-CNTs-LiOH·H₂O-2, and 3D-GO-CNTs-LiOH·H₂O-3, respectively. The peaks at 22.1°, 24.9°, 30.1°, 32.2°, 33.6°, 34.8°, 37.3°, 40.1°, 41.6°, 43.5°, 49.4°, 51.4°, 52.5°, 55.6°, 56.9°, 59.5°, 62.0°, 64.3°, 65.5°, 66.7°, 68.0°, 69.4°, 71.0°, 75.4°, and 76.6° are characteristic peaks of LiOH·H₂O. Graphitic carbon could be identified in 3D-GO-CNTs, 3D-GO-CNTs-LiOH·H₂O-1, 3D-GO-CNTs-LiOH·H₂O-2, and 3D-GO-CNTs-LiOH·H₂O-3 by two diffraction peaks at around 25° and 43° [46]. Pristine LiOH·H₂O shows strong diffraction intensities and sharp peaks. While, after compositing with 3D-GO-CNTs, the LiOH·H₂O peaks faded down and widened. This indicated a homogeneous dispersion of LiOH·H₂O inside 3D-GO-CNTs frames. Increased LiOH·H₂O signal at a sequence of 3D-GO-CNTs-LiOH·H₂O-1, 3D-GO-CNTs-LiOH·H₂O-2, and 3D-GO-CNTs-LiOH·H₂O-3 was in good accordance with increased amount of LiOH·H₂O in 3D-GO-CNTs.

Figure 4 shows the SEM images of LiOH·H₂O, 3D-GO-CNTs, 3D-GO-CNTs-LiOH·H₂O-1, 3D-GO-CNTs-LiOH·H₂O-2, and 3D-GO-CNTs-LiOH·H₂O-3, respectively. LiOH·H₂O displays large particle diameters (from 300 nm to 2 μm) (Figure 4(a)). Figure S1 shows EDS analysis of elemental contents of C and O in synthesized GO. It can be found that elemental mass content of C and O is 60% and 32%, respectively. After compositing with 3D-GO-CNTs, LiOH·H₂O nanoparticles could be seen on the surfaces of 3D-GO-CNTs-LiOH·H₂O-1 (Figure 4(b)) and 3D-GO-CNTs-LiOH·H₂O-2 (Figure 4(c)). In addition, plugged CNTs inside the 3D-GO frames could be clearly observed in Figures 4(b)–4(d). This conformed the intact structure of 3D-GO-CNTs. When the LiOH·H₂O content exceeds 39%, the surface of 3D-GO-CNTs frame is partially covered by LiOH·H₂O. At a LiOH·H₂O content of 59 wt.%, increased amount of bigger LiOH·H₂O nanoparticles could be observed on the surface of 3D-GO-CNTs-LiOH·H₂O-3 (Figure 4(d)).

Figures 5(a)–5(d) show the TEM images of LiOH·H₂O, 3D-GO-CNTs-LiOH·H₂O-1, 3D-GO-CNTs-LiOH·H₂O-2, and 3D-GO-CNTs-LiOH·H₂O-3, respectively. As shown in Figure 5(a), the pristine LiOH·H₂O exists in bulk. LiOH·H₂O nanoparticles are homogeneously anchored on the surface of 3D-GO-CNTs (Figure 5(b) and Figure S2). In order to make clear view of LiOH·H₂O nanoparticles of 3D-GO-CNTs-LiOH·H₂O-1, HR-TEM technology was applied (Figure S3). As shown in Figure S3, LiOH·H₂O nanoparticles with the diameter of 5 nm could be seen and pointed out with red circles. The purity of CNTs used in the composite materials is 65%, and the diameter is at the range of 10–15 nm (Figure S4). Increased LiOH·H₂O content leads to an augmented particle size of nano-LiOH·H₂O (Figures 5(c)

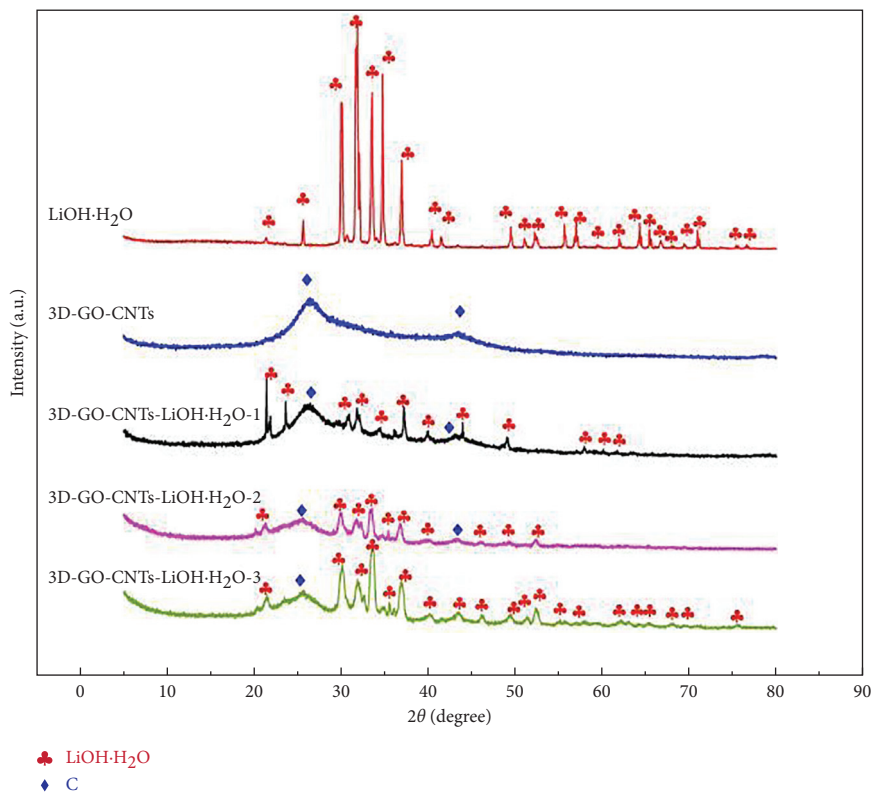


FIGURE 3: XRD spectra of LiOH·H₂O, 3D-GO-CNTs, 3D-GO-CNTs-LiOH·H₂O-1, 3D-GO-CNTs-LiOH·H₂O-2, and 3D-GO-CNTs-LiOH·H₂O-3.

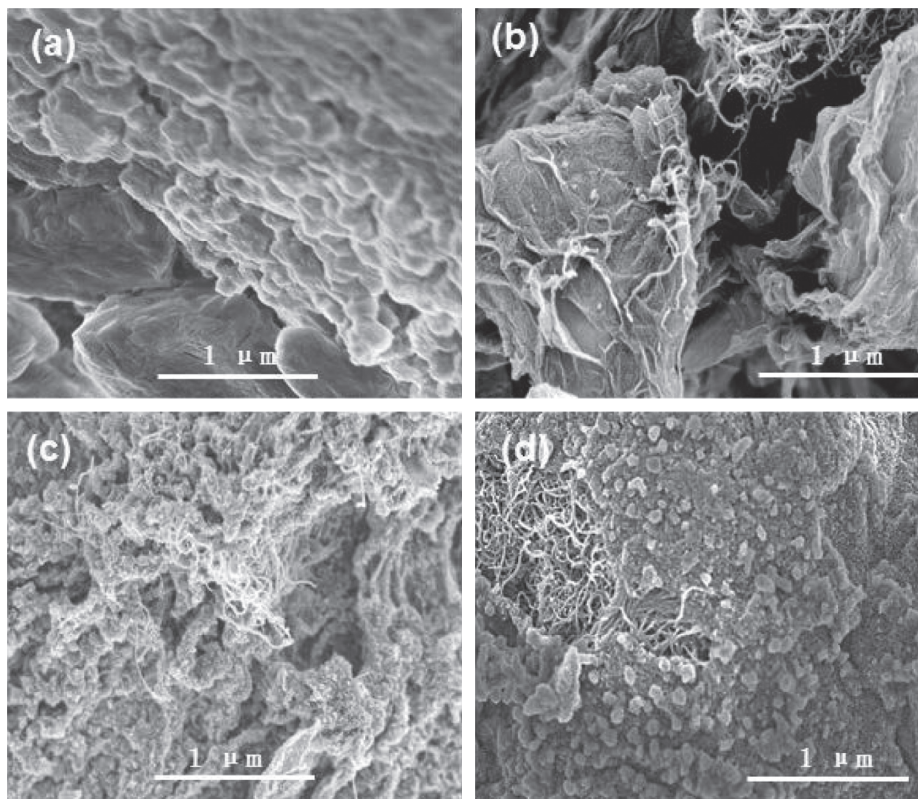


FIGURE 4: SEM images of (a) LiOH·H₂O, (b) 3D-GO-CNTs-LiOH·H₂O-1, (c) 3D-GO-CNTs-LiOH·H₂O-2, and (d) 3D-GO-CNTs-LiOH·H₂O-3.

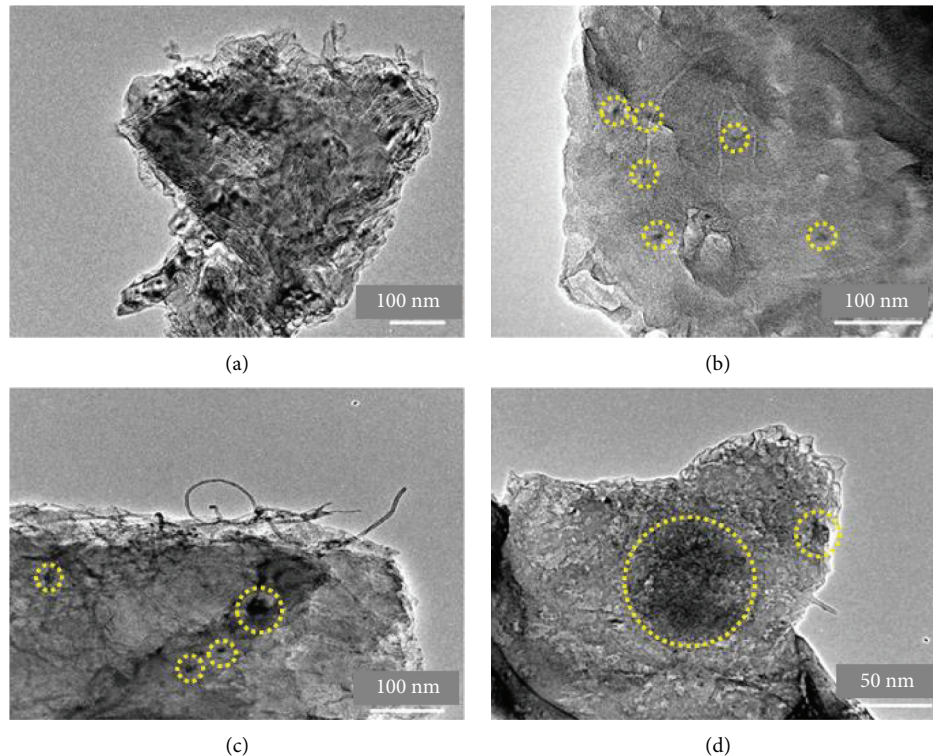


FIGURE 5: TEM images of (a) $\text{LiOH}\cdot\text{H}_2\text{O}$, (b) 3D-GO-CNTs- $\text{LiOH}\cdot\text{H}_2\text{O}$ -1, (c) 3D-GO-CNTs- $\text{LiOH}\cdot\text{H}_2\text{O}$ -2 and (d) 3D-GO-CNTs- $\text{LiOH}\cdot\text{H}_2\text{O}$ -3.

and 5(d)). A maximum size of 50 nm of $\text{LiOH}\cdot\text{H}_2\text{O}$ could be found at a $\text{LiOH}\cdot\text{H}_2\text{O}$ concentration of 59 wt.% (Figure 5(d)).

3D-GO-CNTs frame with affluent oxygen-containing functional groups allows intermolecular hydrogen bond forming [51–53] between the 3D-GO-CNTs frames and $\text{LiOH}\cdot\text{H}_2\text{O}$ nanoparticles. Thus, $\text{LiOH}\cdot\text{H}_2\text{O}$ nanoparticles could be homogeneously dispersed inside 3D-GO-CNTs frame. However, further increased $\text{LiOH}\cdot\text{H}_2\text{O}$ amount will exceed the capacity of 3D-GO-CNTs, which results in an augmented particle size of $\text{LiOH}\cdot\text{H}_2\text{O}$.

The adsorption properties of all samples were examined by nitrogen adsorption-desorption experiment and summarized in Figure 6 and Table 1. The introduction of porous 3D-GO-CNTs frame can significantly increase the specific surface area of the $\text{LiOH}\cdot\text{H}_2\text{O}$ (from $15\text{ m}^2/\text{g}$ to lowest $219\text{ m}^2/\text{g}$). Agreed well with the SEM and TEM results, a larger specific surface area facilitates the homogeneous dispersion of $\text{LiOH}\cdot\text{H}_2\text{O}$ in the 3D-GO-CNTs frame.

3.2. Heat Storage Performance. Figure 7 shows the heat storage performance of LiOH , 3D-GO-CNTs- LiOH -1, 3D-GO-CNTs- LiOH -2, and 3D-GO-CNTs- LiOH -3 after hydration for 1 h. The heat storage density of pristine $\text{LiOH}\cdot\text{H}_2\text{O}$ was 661 kJ/kg due to its slow hydration rate (Figure 7(c)). Figures 7(a) and 7(b) provide the TG and DSC of 3D-GO-CNTs-modified $\text{LiOH}\cdot\text{H}_2\text{O}$, respectively. LiOH was completely converted into $\text{LiOH}\cdot\text{H}_2\text{O}$ after 1 h hydration for all 3D-GO-CNTs- LiOH samples. Highest heat

storage density of 2800 kJ/kg could be achieved for 3D-GO-CNTs- $\text{LiOH}\cdot\text{H}_2\text{O}$ -1 (taking $\text{LiOH}\cdot\text{H}_2\text{O}$ content as a benchmark). The heat storage densities of 3D-GO-CNTs- $\text{LiOH}\cdot\text{H}_2\text{O}$ -2 and 3D-GO-CNTs- $\text{LiOH}\cdot\text{H}_2\text{O}$ -3 were 2051 kJ/kg and 1983 kJ/kg , respectively. Boosted heat storage capacity of 3D-GO-CNTs- $\text{LiOH}\cdot\text{H}_2\text{O}$ compared with that of pristine $\text{LiOH}\cdot\text{H}_2\text{O}$ was due to the enhanced available reaction surface area of $\text{LiOH}\cdot\text{H}_2\text{O}$ nanoparticles inside 3D-GO-CNTs frames. Affluent hydrophilic oxygen-containing functional groups (easy adsorption by water molecular) on the 3D-GO-CNTs surfaces facilitate the homogeneous growing of $\text{LiOH}\cdot\text{H}_2\text{O}$ nanoparticles. Significantly enhanced specific surface areas of 3D-GO-CNTs- $\text{LiOH}\cdot\text{H}_2\text{O}$ due to the adding of 3D-GO-CNTs frames also contributes to this boosted heat storage capacity.

Higher $\text{LiOH}\cdot\text{H}_2\text{O}$ content accompanied with lower heat storage capacity of 3D-GO-CNTs- $\text{LiOH}\cdot\text{H}_2\text{O}$ seems contradictory to the increased amount of $\text{LiOH}\cdot\text{H}_2\text{O}$ which dominates the heat storage capacity. While note that the thermal conductivity of bulk $\text{LiOH}\cdot\text{H}_2\text{O}$ is very poor (Figure 8(b)). This implies that $\text{LiOH}\cdot\text{H}_2\text{O}$ could not be completely decomposed after heating. The increased size of $\text{LiOH}\cdot\text{H}_2\text{O}$ nanoparticles will make the decomposition of internal $\text{LiOH}\cdot\text{H}_2\text{O}$ molecules inside them more difficult. Decreased specific surface areas which leads to smaller evaporation area of dispersed $\text{LiOH}\cdot\text{H}_2\text{O}$ nanoparticles in 3D-GO-CNTs- $\text{LiOH}\cdot\text{H}_2\text{O}$ should also be considered. These two reasons explain clearly for the decreased heat storage capacity with increased $\text{LiOH}\cdot\text{H}_2\text{O}$ content ratio.

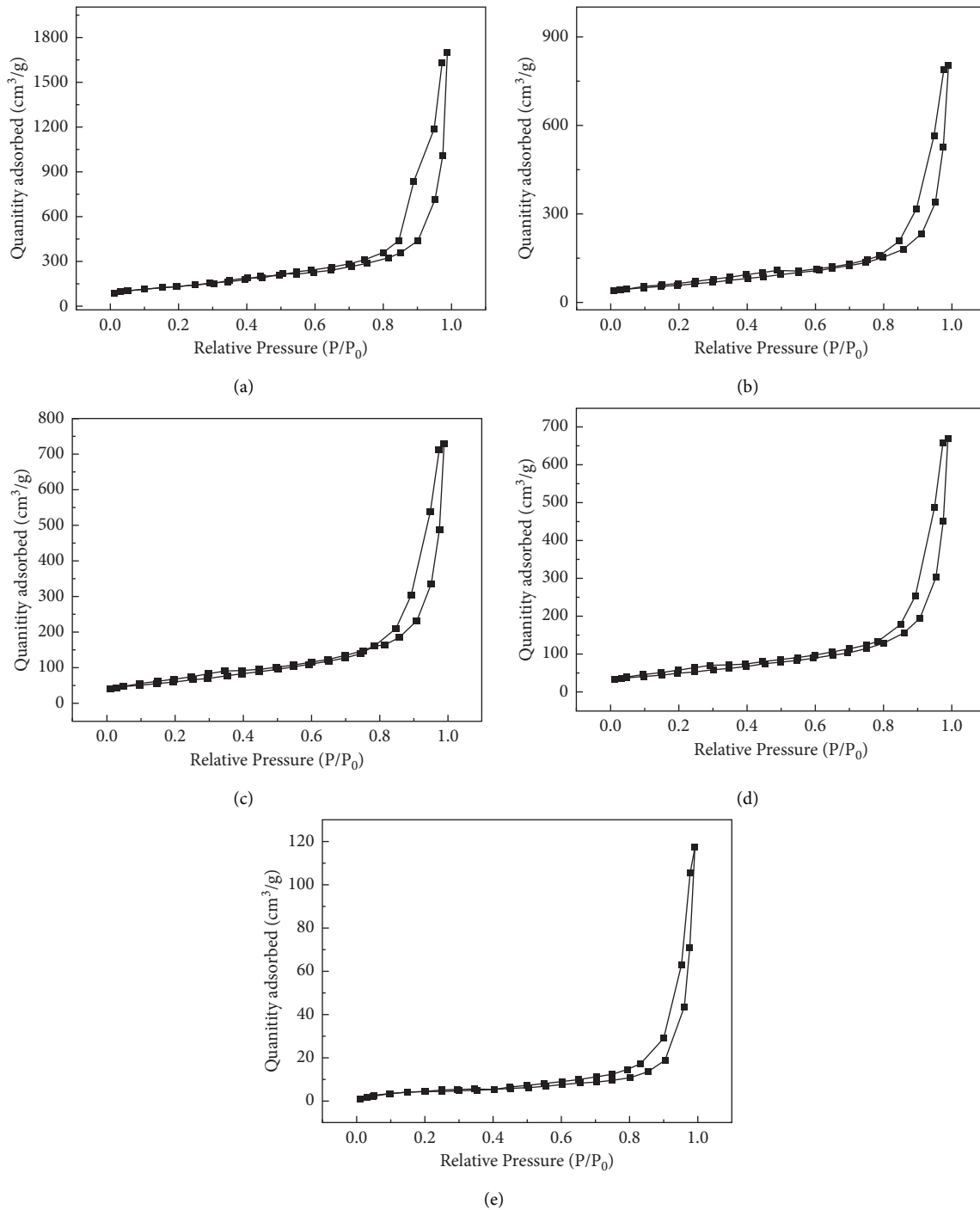


FIGURE 6: N₂ sorption isotherms of (a) 3D-GO-CNTs; (b) 3D-GO-CNTs-LiOH·H₂O-1; (c) 3D-GO-CNTs-LiOH·H₂O-2; (d) 3D-GO-CNTs-LiOH·H₂O-3; (e) LiOH·H₂O.

TABLE 1: BET parameters of 3D-GO-CNTs-LiOH·H₂O and LiOH·H₂O.

Sample name	Specific surface area (m ² /g)	Pore volume (mL/g)	Average pore size (nm)
3D-GO-CNTs	467	0.25	10.12
3D-GO-CNTs-LiOH·H ₂ O-1	219	0.12	1.20
3D-GO-CNTs-LiOH·H ₂ O-2	213	0.11	1.99
3D-GO-CNTs-LiOH·H ₂ O-3	182	0.09	0.99
LiOH·H ₂ O	15	0.06	1.75

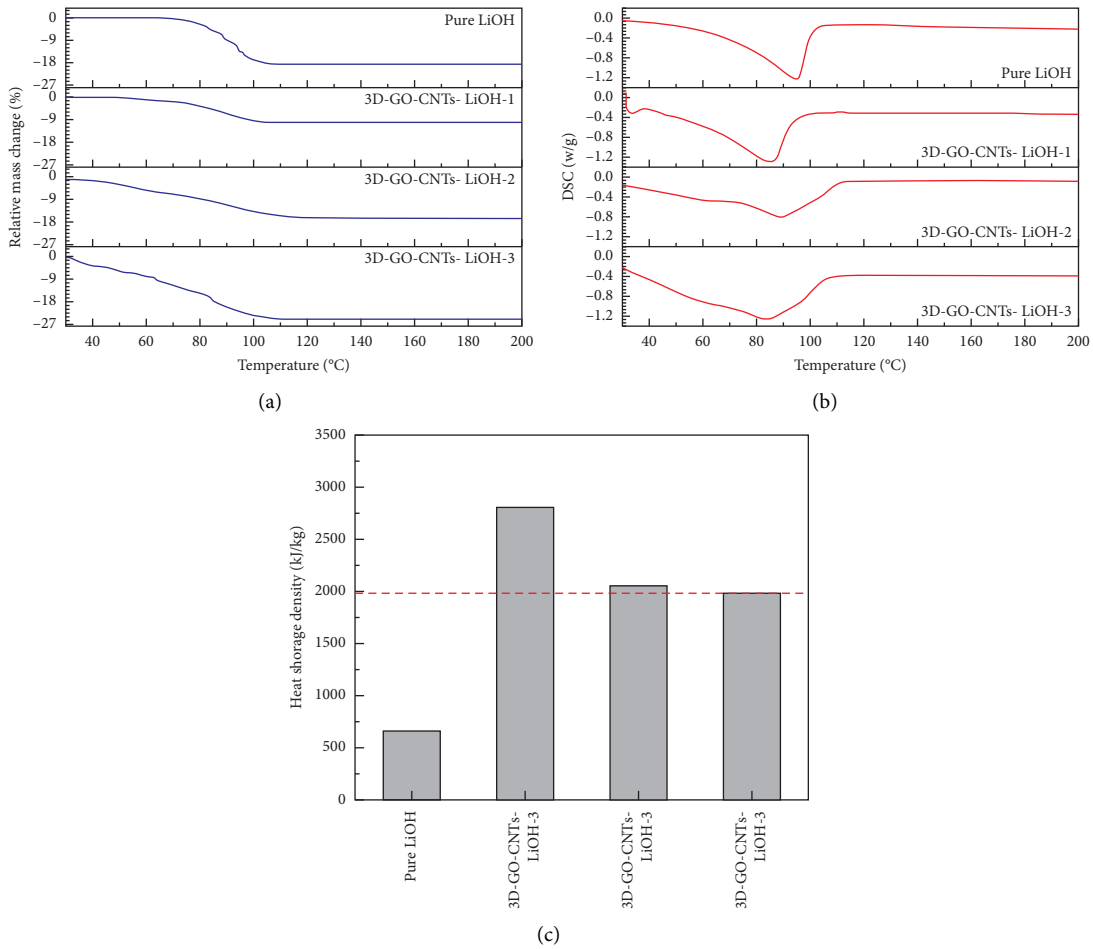


FIGURE 7: TG-DSC test of LiOH, 3D-GO-CNTs-LiOH-1, 3D-GO-CNTs-LiOH-2, and 3D-GO-CNTs-LiOH-3 after hydration for 1 h: (a) TGA; (b) DSC; (c) calculated heat storage density.

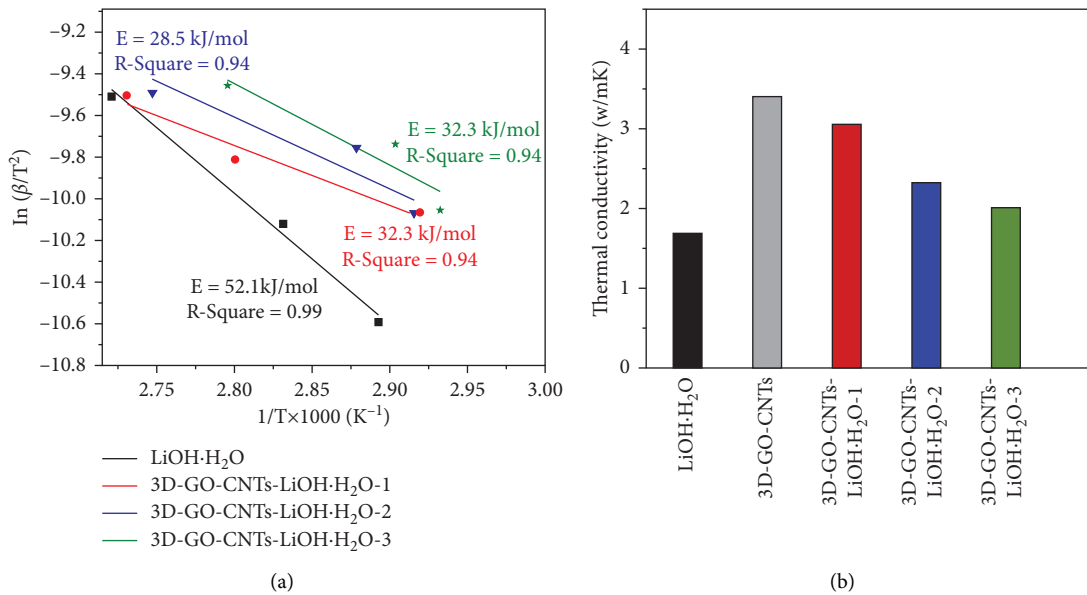


FIGURE 8: (a) Activation energy of dehydration reaction of LiOH·H₂O, 3D-GO-CNTs, 3D-GO-CNTs-LiOH·H₂O-1, 3D-GO-CNTs-LiOH·H₂O-2, and 3D-GO-CNTs-LiOH·H₂O-3; (b) thermal conductivity of LiOH·H₂O, 3D-GO-CNTs, 3D-GO-CNTs-LiOH·H₂O-1, 3D-GO-CNTs-LiOH·H₂O-2, and 3D-GO-CNTs-LiOH·H₂O-3.

The dehydration activation energy of all samples is shown in Figure 8. The activation energy is 52.1 kJ/mol, 23.8 kJ/mol, 28.5 kJ/mol, and 32.3 kJ/mol for LiOH·H₂O, 3D-GO-CNTs-LiOH·H₂O-1, 3D-GO-CNTs-LiOH·H₂O-2, and 3D-GO-CNTs-LiOH·H₂O-3, respectively. The significantly lowered activation energy of 3D-GO-CNTs-LiOH·H₂O than pristine LiOH·H₂O is first due to the increased molar surface energy of LiOH·H₂O nanoparticles [54–56]. And, the high affinity to water molecules of hydrophilic 3D-GO-CNTs frames will increase the colliding frequency between water molecule and LiOH and thus decrease the reaction activation energy. Due to the augmentation effect of 3D-GO-CNTs on specific surface area, the dehydration of LiOH·H₂O nanoparticles became easier during the heating.

After composited with 3D-GO-CNTs frames, the thermal conductivity of LiOH·H₂O was prominently increased (Figure 8(b)). The highest thermal conductivity of 3D-GO-CNTs-LiOH·H₂O was 3.06 W/mK, which was 1.8 times higher than that of pristine LiOH·H₂O. With the increase of LiOH·H₂O capacity, the thermal conductivity decreased. 3D-GO-CNTs-LiOH·H₂O-1 had the highest thermal conductivity and the highest heat storage density, which proved that 3D-GO-CNTs frame can greatly improve the thermal conductivity of pristine LiOH·H₂O, thus boosting the heat storage performance of LiOH·H₂O.

4. Conclusions

Cellulose-originated 3D-GO-CNTs-LiOH·H₂O composite was fabricated using a hydrothermal method. The effects of the amount of LiOH·H₂O on the morphology and heat storage performance of 3D-GO-CNTs-LiOH·H₂O were systematically investigated. The LiOH·H₂O could be homogeneous dispersed inside the 3D-GO-CNTs frames with the size spanning from 5 to 50 nm. Increased content ratios of LiOH·H₂O augment the average size of dispersed LiOH·H₂O nanoparticles. The performance of composite materials was better than pure LiOH·H₂O (activation energy: 52.1 kJ/mol, thermal conductivity: 1.69 W/m·K, and heat storage capacity: 661 kJ/kg). 3D-GO-CNTs-LiOH·H₂O-2 (activation energy: 28.5 kJ/mol, thermal conductivity: 2.33 W/m·K, and heat storage capacity: 2051 kJ/kg); 3D-GO-CNTs-LiOH·H₂O-3 (activation energy: 32.3 kJ/mol, thermal conductivity: 2.01 W/m·K, and heat storage capacity: 1983 kJ/kg). The highest heat storage capacity of 2800 kJ/kg and maximum thermal conductivity of 3.06 W/m·K could be achieved for 3D-GO-CNTs-LiOH·H₂O-1 composite at a LiOH·H₂O content ratio of 23%. Corresponding hydration activation energy decreased sharply from 52.1 kJ/mol (LiOH·H₂O) to 23.8 kJ/mol due to the high hydrophilic property and surface effect of 3D-GO-CNTs frames.

Data Availability

The data used to support the findings of this study are included within the article.

Additional Points

Cellulose-originated 3D-GO-CNTs-LiOH·H₂O composites were synthesized. LiOH·H₂O nanoparticles (5–50 nm) were homogeneously dispersed inside 3D-GO-CNTs frame. LiOH·H₂O content ratio of 23% results in best heat storage performance. Introduction of 3D-GO-CNTs frames provided a new strategy to boost the heat storage performance of LiOH·H₂O.

Conflicts of Interest

The authors declare that they have no conflicts of interest.

Acknowledgments

This study was funded by the National Key Research and Development Program of China (Grant no. SQ2019YFC190252).

Supplementary Materials

Figure S1. EDS analysis of elemental contents of C and O in synthesized GO. Figure S2. SEM image of 3D-GO-CNTs-LiOH·H₂O-3 composite materials. Figure S3. HR-TEM analysis of 3D-GO-CNTs-LiOH·H₂O-1 composite materials. Figure S4. TEM image of synthesized CNTs. (Supplementary Materials)

References

- [1] M. Asif, Y. Tan, L. Pan et al., "Synthesis of a highly efficient 3D graphene-CNT-MnO₂-PANI nanocomposite as a binder free electrode material for supercapacitors," *Physical Chemistry Chemical Physics*, vol. 18, no. 38, pp. 26854–26864, 2016.
- [2] C. Bie, B. Zhu, F. Xu, L. Zhang, and J. Yu, "In situ grown monolayer N-doped graphene on CdS hollow spheres with seamless contact for photocatalytic CO₂ reduction," *Advanced Materials*, vol. 31, no. 42, Article ID 1902868, 2019.
- [3] Q. Cao, S.-J. Han, G. S. Tulevski, Y. Zhu, D. D. Lu, and W. Haensch, "Arrays of single-walled carbon nanotubes with full surface coverage for high-performance electronics," *Nature Nanotechnology*, vol. 8, no. 3, pp. 180–186, 2013.
- [4] X. Cao, Y. Shi, W. Shi et al., "Preparation of novel 3D graphene networks for supercapacitor applications," *Small*, vol. 7, no. 22, pp. 3163–3168, 2011.
- [5] J. Chen, X. Gui, Z. Lin et al., "Pulsed ultra-violet laser interactions with ultra-low-density porous carbon nanotube sponges," *Carbon*, vol. 93, pp. 604–610, 2015.
- [6] Z. Cui, Y. Xue, L. Xiao, and T. Wang, "Effect of particle size on activation energy for thermal decomposition of nano-CaCO₃," *Journal of Computational and Theoretical Nanoscience*, vol. 10, no. 3, pp. 569–572, 2013.
- [7] J. P. Da Cunha and P. Eames, "Compact latent heat storage decarbonisation potential for domestic hot water and space heating applications in the UK," *Applied Thermal Engineering*, vol. 134, pp. 396–406, 2018.
- [8] K. Hoang, A. Janotti, and C. G. Van De Walle, "The particle-size dependence of the activation energy for decomposition of lithium amide," *Angewandte Chemie*, vol. 123, no. 43, pp. 10352–10355, 2011.

- [9] S. Hongois, F. Kuznik, P. Stevens, and J.-J. Roux, "Development and characterisation of a new MgSO₄-zeolite composite for long-term thermal energy storage," *Solar Energy Materials and Solar Cells*, vol. 95, no. 7, pp. 1831-1837, 2011.
- [10] H. Ishitobi, K. Uruma, M. Takeuchi, J. Ryu, and Y. Kato, "Dehydration and hydration behavior of metal-salt-modified materials for chemical heat pumps," *Applied Thermal Engineering*, vol. 50, no. 2, pp. 1639-1644, 2013.
- [11] A. A. Khosa and C. Y. Zhao, "Heat storage and release performance analysis of CaCO₃/CaO thermal energy storage system after doping nano silica," *Solar Energy*, vol. 188, pp. 619-630, 2019.
- [12] G. Krese, R. Koželj, V. Stritih, and U. Stritih, "Thermochemical seasonal solar energy storage for heating and cooling of buildings," *Energy and Buildings*, vol. 164, pp. 239-253, 2018.
- [13] M. Kubota, N. Horie, H. Togari, and H. Matsuda, "Improvement of hydration rate of LiOH/LiOH·H₂O reaction for low-temperature thermal energy storage," in *Proceedings of the 2013 Annual Meeting of Japan Society of Refrigerating and Air Conditioning Engineers*, pp. 10-12, Tokyo, Japan, September 2013.
- [14] M. Kubota, S. Matsumoto, H. Matsuda, H. Y. Huang, H. Y. Huang, and Z. H. He, X. X. Yang, "Chemical heat storage with LiOH/LiOH·H₂O reaction for low-temperature heat below 373 K," *Advanced Materials Research*, vol. 953-954, pp. 757-760, 2014.
- [15] X. Yang, S. Li, H. Huang, J. Li, N. Kobayashi, and M. Kubota, "Effect of carbon nanoadditives on lithium hydroxide monohydrate-based composite materials for low temperature chemical heat storage," *Energies*, vol. 10, no. 5, pp. 644-652, 2017.
- [16] K. Kyaw, T. Shibata, F. Watanabe, H. Matsuda, and M. Hasatani, "Applicability of zeolite for CO₂ storage in a CaO-CO₂ high temperature energy storage system," *Energy Conversion and Management*, vol. 38, no. 10-13, pp. 1025-1033, 1997.
- [17] H. Li, L. Liu, and F. Yang, "Covalent assembly of 3D graphene/polypyrrole foams for oil spill cleanup," *Journal of Materials Chemistry*, vol. 1, no. 10, pp. 3446-3453, 2013.
- [18] K. Awasthi, R. Kumar, R. S. Tiwari, and O. N. Srivastava, "Large scale synthesis of bundles of aligned carbon nanotubes using a natural precursor: turpentine oil," *Journal of Experimental Nanoscience*, vol. 5, no. 6, pp. 498-508, 2010.
- [19] X. Li, J. Yu, M. Jaroniec, and X. Chen, "Cocatalysts for selective photoreduction of CO₂ into solar fuels," *Chemical Reviews*, vol. 119, no. 6, pp. 3962-4179, 2019.
- [20] X. C. Liu, Y. Osaka, H. Y. Huang et al., "Development of low-temperature desulfurization performance of a MnO₂/AC composite for a combined SO₂ trap for diesel exhaust," *RSC Advances*, vol. 6, no. 98, pp. 96367-96375, 2016.
- [21] G. Maouris, E. J. Sarabia Escriba, S. Acha, N. Shah, and C. N. Markides, "CO₂ refrigeration system heat recovery and thermal storage modelling for space heating provision in supermarkets: an integrated approach," *Applied Energy*, vol. 264, Article ID 114722, 2020.
- [22] M. Mehrali, S. Tahan Latibari, M. Mehrali, T. M. I. Mahlia, and H. S. Cornelis Metselaar, "Effect of carbon nanospheres on shape stabilization and thermal behavior of phase change materials for thermal energy storage," *Energy Conversion and Management*, vol. 88, pp. 206-213, 2014.
- [23] Y. Meng, T. M. Young, P. Liu, C. I. Contescu, B. Huang, and S. Wang, "Ultralight carbon aerogel from nanocellulose as a highly selective oil absorption material," *Cellulose*, vol. 22, no. 1, pp. 435-447, 2015.
- [24] E. Muñoz-Sandoval, A. J. Cortes-López, B. Flores-Gómez, J. L. Fajardo-Díaz, R. Sánchez-Salas, and F. López-Urías, "Carbon sponge-type nanostructures based on coaxial nitrogen-doped multiwalled carbon nanotubes grown by CVD using benzylamine as precursor," *Carbon*, vol. 115, pp. 409-421, 2017.
- [25] H. Ogura, T. Yamamoto, and H. Kage, "Efficiencies of CaO/H₂O/Ca(OH)₂ chemical heat pump for heat storing and heating/cooling," *Energy*, vol. 28, no. 14, pp. 1479-1493, 2003.
- [26] D. Qiang, M. Zhang, J. Li, H. Xiu, and Q. Liu, "Selective hydrolysis of cellulose for the preparation of microcrystalline cellulose by phosphotungstic acid," *Cellulose*, vol. 23, no. 2, pp. 1199-1207, 2016.
- [27] Y. Shen, D. Sun, L. Yu et al., "A high-capacity lithium-air battery with Pd modified carbon nanotube sponge cathode working in regular air," *Carbon*, vol. 62, pp. 288-295, 2013.
- [28] D. A. Sheppard, M. Paskevicius, and C. E. Buckley, "Thermodynamics of hydrogen desorption from NaMgH₃ and its application as a solar heat storage medium," *Chemistry of Materials*, vol. 23, no. 19, pp. 4298-4300, 2011.
- [29] P. Song, X. Shen, X. He et al., "Cellulose-derived nitrogen-doped hierarchically porous carbon for high-performance supercapacitors," *Cellulose*, vol. 26, no. 2, pp. 1195-1208, 2019.
- [30] X. Su, J. Wu, and B. J. Hinds, "Catalytic activity of ultrathin Pt films on aligned carbon nanotube arrays," *Carbon*, vol. 49, no. 4, pp. 1145-1150, 2011.
- [31] R. Kumar, S. Sahoo, E. Joanni et al., "Recent progress in the synthesis of graphene and derived materials for next generation electrodes of high performance lithium ion batteries," *Progress in Energy and Combustion Science*, vol. 75, pp. 100786-100841, 2019.
- [32] D. Nitika, S. Sumanta, K. Rajesh, and K. S. Rajesh, "A review of the microwave-assisted synthesis of carbon nanomaterials, metal oxides/hydroxides and their composites for energy storage applications," *Nanoscale*, vol. 13, pp. 11679-11711, 2021.
- [33] R. Kumar, R. K. Singh, D. P. Singh, E. Joanni, R. M. Yadav, and S. A. Moshkalev, "Laser-assisted synthesis, reduction and micro-patterning of graphene: recent progress and applications," *Coordination Chemistry Reviews*, vol. 342, pp. 34-79, 2017.
- [34] R. Kumar, E. Joanni, R. K. Singh, D. P. Singh, and S. A. Moshkalev, "Recent advances in the synthesis and modification of carbon-based 2D materials for application in energy conversion and storage," *Progress in Energy and Combustion Science*, vol. 67, pp. 115-157, 2018.
- [35] R. Kumar, S. Sahoo, E. Joanni et al., "Heteroatom doped graphene engineering for energy storage and conversion," *Materials Today*, vol. 39, pp. 47-65, 2020.
- [36] R. Kumar, M. M. Abdel-Galeil, K. Z. Ya et al., "Facile and fast microwave-assisted formation of reduced graphene oxide-wrapped manganese cobaltite ternary hybrids as improved supercapacitor electrode material," *Applied Surface Science*, vol. 481, pp. 296-306, 2019.
- [37] R. Kumar, S. Sahoo, W. K. Tan, G. Kawamura, A. Matsuda, and K. K. Kar, "Microwave-assisted thin reduced graphene oxide-cobalt oxide nanoparticles as hybrids for electrode materials in supercapacitor," *Journal of Energy Storage*, vol. 40, pp. 102724-102732, 2021.
- [38] R. Kumar, R. K. Singh, A. K. Singh, A. R. Vaz, C. S. Rout, and S. A. Moshkalev, "Facile and single step synthesis of three dimensional reduced graphene oxide-NiCoO₂ composite

- using microwave for enhanced electron field emission properties,” *Applied Surface Science*, vol. 416, pp. 259–265, 2017.
- [39] R. Kumar, R. K. Singh, J. Singh, R. S. Tiwari, and O. N. Srivastava, “Synthesis, characterization and optical properties of graphene sheets-ZnO multipod nanocomposites,” *Journal of Alloys and Compounds*, vol. 526, pp. 129–134, 2012.
- [40] H. Hashtroudi, R. Kumar, R. Savu et al., “Hydrogen gas sensing properties of microwave-assisted 2D Hybrid Pd/rGO: effect of temperature, humidity and UV illumination,” *International Journal of Hydrogen Energy*, vol. 46, no. 10, pp. 7653–7665, 2021.
- [41] I. S. El-Hallag, M. N. El-Nahass, S. M. Youssry, R. Kumar, M. M. Abdel-Galeil, and A. Matsuda, “Facile in-situ simultaneous electrochemical reduction and deposition of reduced graphene oxide embedded palladium nanoparticles as high performance electrode materials for supercapacitor with excellent rate capability,” *Electrochimica Acta*, vol. 314, pp. 124–134, 2019.
- [42] R. Kumar, S. Sahoo, E. Joanni et al., “Recent progress on carbon-based composite materials for microwave electromagnetic interference shielding,” *Carbon*, vol. 177, pp. 304–331, 2021.
- [43] Q. Wang, Y. Lei, Z. Chen et al., “Fe/Fe₃C@C nanoparticles encapsulated in N-doped graphene-CNTs framework as an efficient bifunctional oxygen electrocatalyst for robust rechargeable Zn-air batteries,” *Journal of Materials Chemistry*, vol. 6, no. 2, pp. 516–526, 2018.
- [44] Y. Wen, M. Jiang, C. L. Kitchens, and G. Chumanov, “Synthesis of carbon nanofibers via hydrothermal conversion of cellulose nanocrystals,” *Cellulose*, vol. 24, no. 11, pp. 4599–4604, 2017.
- [45] J. Wang, H. Xie, Z. Xin, Y. Li, and L. Chen, “Enhancing thermal conductivity of palmitic acid based phase change materials with carbon nanotubes as fillers,” *Solar Energy*, vol. 84, no. 2, pp. 339–344, 2010.
- [46] X. Yang, S. Li, S. Zhang, X. Chen, and S. Peng, “Facile assembly of cellulose-derived 3D-graphene/lithium hydroxide monohydrate nanocomposite for low-temperature chemical heat storage,” *Cellulose*, vol. 26, no. 8, pp. 4815–4825, 2019.
- [47] R. Kumar, R. K. Singh, P. K. Dubey, D. P. Singh, and R. M. Yadav, “Self-assembled hierarchical formation of conjugated 3D cobalt oxide nanobead-CNT-graphene nanostructure using microwaves for high-performance supercapacitor electrode,” *ACS Applied Materials & Interfaces*, vol. 7, no. 27, pp. 15042–15051, 2015.
- [48] G. Whiting, D. Grondin, S. Bennici, and A. Auroux, “Heats of water sorption studies on zeolite-MgSO₄ composites as potential thermochemical heat storage materials,” *Solar Energy Materials and Solar Cells*, vol. 112, pp. 112–119, 2013.
- [49] W. Wongsuwan, S. Kumar, P. Neveu, and F. Meunier, “A review of chemical heat pump technology and applications,” *Applied Thermal Engineering*, vol. 21, no. 15, pp. 1489–1519, 2001.
- [50] X. Yang, H. Huang, Z. Wang, M. Kubota, Z. He, and N. Kobayashi, “Facile synthesis of graphene oxide-modified lithium hydroxide for low-temperature chemical heat storage,” *Chemical Physics Letters*, vol. 644, pp. 31–34, 2016.
- [51] Z. Yc, “Effect of diameter on apparent activation energy of non-isothermal decomposition reaction of nano-Mg (OH)₂ powder,” *Current Nanoscience*, vol. 8, pp. 97–101, 2012.
- [52] D. Yuan, J. Chen, J. Zeng, and S. Tan, “Preparation of monodisperse carbon nanospheres for electrochemical capacitors,” *Electrochemistry Communications*, vol. 10, no. 7, pp. 1067–1070, 2008.
- [53] Y. Yuan, Y. Li, L. Duan, H. Liu, J. Zhao, and Z. Wang, “CaO/Ca(OH)₂ thermochemical heat storage of carbide slag from calcium looping cycles for CO₂ capture,” *Energy Conversion and Management*, vol. 174, pp. 8–19, 2018.
- [54] Z. Zeng, X. Gui, Z. Lin et al., “Carbon nanotube sponge-array tandem composites with extended energy absorption range,” *Advanced Materials*, vol. 25, no. 8, pp. 1185–1191, 2013.
- [55] K. Zhang, T. Li, L. Ling et al., “Facile synthesis of high density carbon nanotube array by a deposition-growth-densification process,” *Carbon*, vol. 114, pp. 435–440, 2017.
- [56] L.-M. Zhang, X.-L. Sui, L. Zhao, G.-S. Huang, D.-M. Gu, and Z.-B. Wang, “Three-dimensional hybrid aerogels built from graphene and polypyrrole-derived nitrogen-doped carbon nanotubes as a high-efficiency Pt-based catalyst support,” *Carbon*, vol. 121, pp. 518–526, 2017.